Downloaded from http://sp.lyellcollection.org/ at Universiteitsbibliotheek Utrecht on October 27, 2015

Compaction creep of simulated anhydrite fault gouge by pressure solution: theory v. experiments and implications for fault sealing

A. M. H. PLUYMAKERS* & C. J. SPIERS

HPT Laboratory, Department of Earth Sciences, Faculty of Geosciences, Utrecht University, Budapestlaan 4, 3584 CD, The Netherlands

**Corresponding author (e-mail: A.M.H.Pluymakers@uu.nl)*

Abstract: The sealing and healing behaviour of faults filled with anhydrite gouge, by processes such as pressure solution, is of interest in relation both to the integrity of faults cutting geological storage systems sealed by anhydrite caprocks and to seismic events that may nucleate in anhydrite-bearing sequences, such as those present in the seismogenic zone beneath the Apennines. We have developed a detailed series of kinetic models for pressure solution in anhydrite fault gouge, allowing for dissolution, diffusion and precipitation control, to estimate the time scale on which such sealing and healing effects occur. We compare the models obtained with previously reported experimental data on compaction creep rates in simulated anhydrite fault gouge, tested under wet, upper crustal conditions. The results confirm earlier indications that compaction under these conditions likely occurs by diffusion-controlled pressure solution. Applying our most rigorous model for diffusion-controlled pressure solution, constrained by the fit to the experimental data, we infer that anhydrite fault sealing will occur in a few decades at most, which is rapid compared with both CO_2 storage time scales and with the recurrence interval for seismicity in the Apennines.

Fault rock transport properties, such as permeability and capillary entry pressure, form a subject of major interest in crustal geoscience. First, they play a key role in controlling natural trapping of oil, gas and hydrothermal minerals, the latter via fault-valve behaviour for example. Second, they are central to determining the containment integrity of geological storage systems for fluids such as CO_2, natural gas and hydrogen fuel, notably when the storage reservoir is laterally sealed by faults. Third, fault rock permeability, its spatial distribution and its temporal evolution exert a profound influence on fault zone fluid pressures and hence strength throughout the seismic cycle of active faults (e.g. Sibson 1992; Faulkner & Rutter 2001; Wibberley & Shimamoto 2003; Wibberley *et al.* 2008; Faulkner *et al.* 2010; Chen *et al.* 2013).

When faults are inactive, fault rocks are generally expected to compact and heal by processes such as diffusive mass transfer, leading to strength recovery and a reduction in fault zone permeability (e.g. Angevine *et al.* 1982). Upon fault reactivation due to tectonic loading, to fluid over-pressuring or to stress changes induced by subsurface exploitation activities, new fault zone damage and fault gouge may be formed, increasing porosity and permeability (Hickman *et al.* 1995; Rutqvist *et al.* 2013). When fault motion once again ceases, a new cycle will be initiated in which the newly formed gouge will compact, heal and seal as a function of time. To estimate the time scales over which such effects take place, an understanding of the deformation mechanisms that control fault (gouge) compaction, healing and sealing is needed.

In this study we address these compaction and sealing processes for anhydrite gouge in particular, which is currently of special interest in relation to two of the three reasons listed above. Many hydrocarbon reservoirs and many potential CO_2 storage reservoirs are sealed by (faulted) anhydrite or interbedded anhydrite-carbonate caprocks. Examples of major reservoir systems topped partly or wholly by such sequences include the onshore Rotliegend gas fields of the Netherlands (Glennie 2001), many of the Qatar gas fields (which contain *c.* 14% of the global gas supply; Oil & Gas Journal 2013), the K12-b CO_2 storage pilot-site in the Dutch North Sea (Vandeweijer *et al.* 2011) and the (onshore) CO_2 injection field at Weyburn in Canada (Cantucci *et al.* 2009). Additionally, much of the highly damaging seismicity experienced in the Italian Apennines in recent years involves rupture nucleation in the anhydrite-carbonate cover sequence that characterizes the Apennines region (De Paola *et al.* 2008; Mirabella *et al.* 2008; Collettini *et al.* 2009; Trippetta *et al.* 2010).

Motivated by these considerations, Pluymakers *et al.* (2014) recently performed uniaxial compaction experiments on simulated anhydrite fault gouge with different initial mean grain sizes (d = 20–500 μm), under both dry and wet conditions, at near *in situ* temperatures and stresses, that is, at

From: Faulkner, D. R., Mariani, E. & Mecklenburgh, J. (eds) 2015. *Rock Deformation from Field, Experiments and Theory: A Volume in Honour of Ernie Rutter*. Geological Society, London, Special Publications, **409**, 107–124. First published online August 8, 2014, http://dx.doi.org/10.1144/SP409.6
© The Geological Society of London 2015. Publishing disclaimer: www.geolsoc.org.uk/pub_ethics

Downloaded from http://sp.lyellcollection.org/ at Universiteitsbibliotheek Utrecht on October 27, 2015

80 °C, effective axial stresses of 5–12 MPa and pore fluid pressures of 15 MPa (or else 0.1 MPa, i.e. atmospheric pressure for control purposes). For a detailed description of the one-dimensional (1D) compaction vessel and method used, refer to Schutjens (1991), Hangx *et al.* (2010), Zhang *et al.* (2010) and Pluymakers *et al.* (2014). All samples were first lightly pre-compacted to obtain a more or less constant porosity (ϕ_{0C}) prior to initiating creep testing (see also Niemeijer *et al.* 2002; Hangx *et al.* 2010). Relatively low axial effective stresses were chosen for subsequent creep testing to minimize any instantaneous compaction by grain breakage, thus maintaining known initial grain size and keeping the porosity high enough to allow creep rates to be measured on a reasonable time scale (typically 1–3 weeks).

In these experiments, Pluymakers *et al.* found that samples loaded in the presence of a pre-saturated solution phase crept at easily measurable rates, whereas dry samples showed negligible creep. This implies that fluid-assisted processes controlled anhydrite compaction and that plasticity played a negligible role under the experimental conditions. Interestingly, samples tested wet, that is, in the presence of the solution phase, showed two compaction regimes (see Fig. 1). At fine grain sizes (grain diameter <70 μm), deformation rates measured at constant applied stress and specific porosity values showed an inverse dependence on grain size with a sensitivity (grain size exponent) close to -3 (Fig. 1) and a low stress sensitivity of strain rate. This, plus retardation of creep observed upon addition of a precipitation reaction (i.e. scale) inhibitor, along with microstructural evidence for solution transfer with little or no grain size reduction, suggested diffusion-controlled pressure solution as the controlling mechanism of compaction in this fine grain size regime (cf. pressure solution in NaCl or calcite; Spiers & Schutjens 1990; Zhang *et al.* 2010; Liteanu *et al.* 2012). With increasing grain size, this behaviour gave way to a regime showing a direct dependence of creep rate on grain size (Fig. 1). Microstructural evidence for grain scale brittle failure and grain size reduction, and a high stress sensitivity of strain rate visible in the mechanical data, led to the conclusion that for these coarse-grained samples (grain diameter >200 μm) deformation was controlled mainly by a subcritical microcracking mechanism (cf. Liteanu *et al.* 2012 for calcite). The two regimes were separated by a transition region, in which the stress and grain size

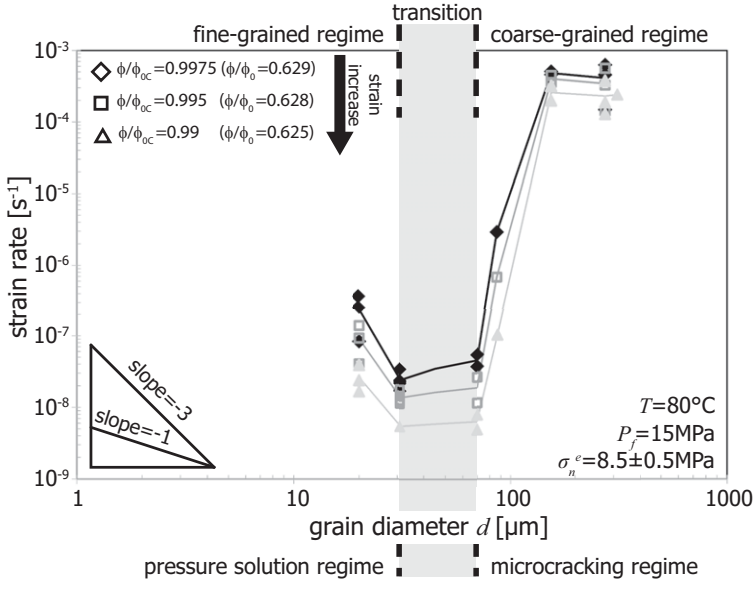

Fig. 1. Strain rate measured at fixed normalized porosity ϕ/ϕ_{0C} v. grain size, as reported by Pluymakers *et al.* (2014), for 1D compaction of simulated anhydrite fault gouge tested wet at an applied effective stress (σ_n^e) of 8.5 ± 0.5 MPa and an upper crustal reservoir temperature of 80 °C. Errors in log strain rate fall (just) within the symbol size. Fine-grained samples show a negative grain size dependence with a slope around −3, transitioning towards a strong positive grain size dependence at grain sizes >70 μm. Note that ϕ represents sample porosity at a given instant during creep of the samples, while ϕ_{0C} is a normalizing porosity measured at the initiation of creep. Porosities ϕ, normalized with respect to the porosity ϕ_0 of a simple cubic pack of spheres, are also given for later comparison with model calculations.

Downloaded from http://sp.lyellcollection.org/ at Universiteitsbibliotheek Utrecht on October 27, 2015

dependence of strain rate indicate mixed pressure solution and subcritical microcracking mechanisms. Despite this complexity, it was argued by Pluymakers *et al.* (2014) that fault (re)activation would generally produce a fine cataclastic gouge with a grain size falling in the fine regime, and that pressure solution would therefore control subsequent gouge compaction. However, only a qualitative comparison was made with pressure solution models.

In the current paper, we make a detailed, quantitative comparison between the above experimental results obtained for the fine-grained creep regime (Fig. 1) and kinetic models for pressure solution. To do this, we first develop a series of models for compaction creep by pressure solution that are useful for understanding fault rock compaction properties in a general sense, but can also be compared directly with the results of the compaction experiments on anhydrite reported by Pluymakers *et al.* (2014). These models build upon the classical model for diffusion-controlled pressure solution presented by Rutter (1976) by including the possibility of interfacial reaction control. We go on to use the model that best explains the experimental data reported by Pluymakers *et al.* (2014) to provide an order of magnitude estimate of fault sealing rates and times for anhydrite fault gouge compacting at *in situ* crustal conditions, and consider the implications for anhydrite-capped CO_2 storage systems and for the seismic cycle in the anhydrite-carbonate cover sequences of the Italian Apennines.

A model for fault gouge compaction by pressure solution creep

Pioneered by Ernie Rutter (Rutter 1976, 1983), numerous models have been developed for the kinetics of deformation and compaction creep of porous granular rock/mineral aggregates by pressure solution (Raj 1982; Lehner 1990, 1995; Spiers & Schutjens 1990; Shimizu 1995; Renard *et al.* 1997; Schutjens & Spiers 1999; Gundersen *et al.* 2002; Spiers *et al.* 2004). However, these models frequently ignore the possibility of dissolution or precipitation as a rate-controlling mechanism, focusing instead on grain boundary diffusion control (e.g. Rutter 1976; Schutjens & Spiers 1999). In the case of sparingly and poorly soluble ionic solids, such as gypsum or calcite, both dissolution and precipitation are known to limit pressure solution rates under certain conditions (see De Meer & Spiers 1997; Zhang *et al.* 2010). In developing pressure solution models for comparison with compaction experiments on fine-grained anhydrite gouge, it is therefore important to consider dissolution, precipitation and grain boundary diffusion as potential rate-controlling processes. For highly porous aggregates with a large molar volume such as anhydrite ($\Omega = 4.6 \times 10^{-5}$ m^3 mol^{-1}) it is also desirable to avoid the (unnecessary) assumption, often made in pressure solution creep models, that normal stresses at grain boundaries are low enough to allow the stress-induced solubility enhancement ($\Delta C/C_0$) that drives pressure solution to be approximated by an asymptotic linear relation of the form $\Delta C/C_0 = \sigma_n^e \Omega/RT$, as opposed to the form $\Delta C/C_0 = [\exp(\sigma_n^e \Omega/RT) - 1]$. Here, ΔC is the absolute enhancement in the solubility of the solid at stressed grain contacts, C_0 is the solubility in the unstressed reference condition (i.e. surrounded by pore fluid at hydrostatic pressure P_f), σ_n^e is the effective normal stress at grain contacts, R is the gas constant and T is the absolute temperature (see Spiers *et al.* 2004). A further step that is useful in a practical sense, is to design models for pressure solution creep using porosity to represent aggregate structure instead of using grain geometry or strain (cf. Spiers & Schutjens 1990; Schutjens 1991; Zhang *et al.* 2010).

In the following, we combine all of these 'refinements' to develop models for compaction creep by dissolution-, diffusion- and precipitation-controlled pressure solution that are suitable for comparison with the experimental data on simulated anhydrite gouge presented by Pluymakers *et al.* (2014).

Microstructural model and driving force

In a granular aggregate, such as a monomineralic fault gouge, loaded in the presence of a pore fluid solution phase, stress-induced differences in chemical potential (hence solubility) between the load-bearing grain contacts and the free pore walls drive material to dissolve at the contacts and to precipitate on the pore wall surfaces (Rutter 1976, 1983; Raj 1982; Lehner 1990, 1995). Let us assume that such an aggregate is composed of a simple cubic pack of spherical grains of uniform size abutting at flat grain-to-grain contacts, with an initially saturated solution filling the open pore space (Fig. 2). We further assume that grain contacts are penetrated by a thin fluid film present in microscopic island-channel form (e.g. Raj 1982; Lehner 1990; Spiers & Schutjens 1990; Paterson 1995), in island-crack form (e.g. Den Brok 1998), or as an adsorbed film (e.g. Rutter 1976). Note here that the form of the grain boundary fluid does not affect the development of a creep model for pressure solution, only the value of the parameters describing the grain boundary properties. Following the derivations given by numerous previous authors (e.g. Paterson 1973; Rutter 1976; Raj 1982; Lehner 1990, 1995; Spiers *et al.* 2004), when an effective stress is applied to the solid framework, the drop in the normal

Downloaded from http://sp.lyellcollection.org/ at Universiteitsbibliotheek Utrecht on October 27, 2015

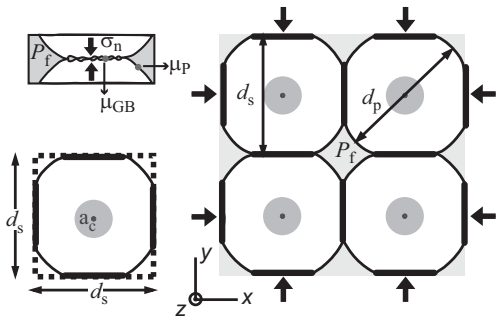

Fig. 2. Aggregate geometry assumed in developing our kinetic model(s) for compaction creep of a granular gouge material. The aggregate is assumed to consist of a simple cubic pack of spheres of uniform size and with flat grain-to-grain contacts, the pores being filled with a pre-saturated solution phase at uniform pressure P_f. The approximation is made that $d_s \approx d$, the equivalent circular grain diameter or grain size. Grain contacts are assumed circular with an area a_c. Note that while we assume a simple cubic grain pack, our analysis is applicable for any packing geometry specifiable in terms of the microstructural parameters F, q and Z as defined in the text.

component of solid chemical potential $\Delta\widetilde{\mu_n}$ between grain contact and pore wall sites is given by

$$\Delta\widetilde{\mu_n} \approx (\widetilde{\sigma_n} - P_f)\Omega \tag{1}$$

where $\widetilde{\sigma_n}$ is the local mean normal stress (MPa) acting on a given grain boundary element (i.e. site) and P_f is the pore fluid pressure (MPa) acting on the free pore walls. Assuming the aggregate is subjected to a total hydrostatic stress P, the normal force balance across any planar grain-to-grain contact area (a_c) leads to the relation $\sigma_n a_c + P_f(d_s{}^2 - a_c) = Pd_s{}^2$, where d_s is the centre-to-centre grain spacing (see Fig. 2) and where σ_n is the average normal stress transmitted across entire grain contacts. Rearranging this leads to $\sigma_n = (P - P_f)(d_s{}^2/a_c) + P_f$, which, setting $\sigma_n^e = P - P_f$ for the applied effective stress and combining with Equation (1), yields

$$\Delta\mu_n \approx \frac{\sigma_n^e \Omega\, d_s{}^2}{a_c} \tag{2}$$

for the average difference in solid chemical potential between grain contacts and pore walls. As an approximation, easily shown (from grain pack geometry) to be reasonable for porosities down to 5–10%, we assume that $d_s = d_p = d$ where d is the sample grain size (e.g. equivalent circular diameter) as measured in a thin section for example; d_s is the truncated diametral grain spacing and d_p is the grain diameter as measured between pore walls (see Fig. 2). We further assume that the mean grain contact area (a_c) can be adequately approximated as a continuous function of porosity $f(\phi)$, via the relation

$$a_c = \frac{Fd^2}{Z} f(\phi) \tag{3}$$

where F is a shape factor of value π for spherical grains (for other shapes, F lies between 2 and 4) and Z is the grain coordination number. For this relation to be sufficiently accurate, $f(\phi)$ should be chosen such that (a) $f(\phi) \to 0$ when $\phi \to \phi_0$, where ϕ_0 is the starting porosity at which grain contacts show negligible contact area, and (b) $f(\phi) \to h$ as $\phi \to 0$, where h is the geometric factor needed to recover the correct value of a_c from Equation (3) when $\phi = 0$. A simple porosity function roughly satisfying these constraints is

$$f(\phi) = \frac{q - 2\phi}{q} \tag{4}$$

where $q = 2\phi_0$ (cf. Spiers *et al.* 2004). Down to porosities of *c.* 5%, this function, with the implicit assumption that $h = 1$, provides a good approximation for a_c as obtained from exact geometric solutions (Gundersen *et al.* 2002; Niemeijer *et al.* 2002). The approximation breaks down at lower porosities however, since, with ongoing solution transfer, the grain geometry rapidly changes from spherical to cubic. Finally, combining Equations (2), (3) and (4) and using our approximation that $d_s \approx d$ leads to the following relation for the mean driving force for pressure solution transfer of mass from grain contacts to pore walls for the present system:

$$\Delta\mu_n \approx \frac{Z}{F}\sigma_n^e \Omega \frac{q}{q - 2\phi}. \tag{5}$$

Rate-controlling steps

Since pressure solution is a serial process, during steady-state mass transfer from grain contacts to pore walls (i.e. in a 'closed' system where there is no long-range exchange of solid mass with the surroundings) the chemical potential drop $\Delta\mu_n$ between source (dissolution) and sink (precipitation) sites is given by the sum $\Delta\mu_n = \Delta\mu_s + \Delta\mu_d + \Delta\mu_p$ (Raj 1982; Paterson 1995; Spiers *et al.* 2004), in which the subscripts s, d and p denote the potential drop or driving force associated with the dissolution, diffusion and precipitation steps respectively. This relation applies at the local source–sink scale (i.e. to $\Delta\widetilde{\mu_n}$) and to the average potential drop between grain contacts and pore walls (i.e. to $\Delta\mu_n$). In the limit when one of the

Downloaded from http://sp.lyellcollection.org/ at Universiteitsbibliotheek Utrecht on October 27, 2015

kinetic steps is the slowest, hence rate controlling, $\Delta\mu_n$ and $\Delta\widetilde{\mu}_n$ will be solely consumed in driving that specific process (Raj 1982; Spiers *et al.* 2004). This is precisely equivalent to the statement (following Lehner 1990) that the total dissipation due to pressure solution creep is the sum of the dissipation due to the kinetic processes operating, that is, to dissolution, diffusion and (in a closed system) precipitation, and that, when one of these processes is rate controlling, then all mechanical work is dissipated by that process (see also Spiers & Schutjens 1990).

Dissolution-controlled compaction creep. Against this background, when dissolution at grain contacts is rate controlling, $\Delta\mu_n \approx \Delta\mu_s \approx (Z/F)\sigma_n^e \Omega[q/(q-2\phi)]$. Assuming a linear dissolution law typical of many minerals (Brantley *et al.* 2008), the dissolution rate in local grain elements (i.e. at local source sites) is given in terms of the velocity $\widetilde{V}_c$(m s^{-1}) of the dissolving interface as $\widetilde{V}_c = \alpha k_+ \Omega\left[(\widetilde{C}_n - \widetilde{C}_f)/\widetilde{C}_f\right]$ (Van Noort & Spiers 2009), where α is a factor allowing for the influence of grain boundary structure on dissolution rate ($\alpha \approx 0.9$, Van Noort & Spiers 2009), k_+ is the geochemical dissolution rate constant for the unstressed solid at the reference pressure P_f (mol m^{-2} s^{-1}), $\widetilde{C}_f$ is the concentration of the dissolved solid in the grain boundary fluid (mol m^{-3}) and $\widetilde{C}_n$ (mol m^{-3}) can be viewed as the mean enhanced solubility of the solid at grain boundary dissolution sites due to the local mean grain boundary stress $\widetilde{\sigma}_n$. Alternatively, we can write $\widetilde{V}_c = I_s(\Delta\widetilde{C}/\widetilde{C}_f)$ where $\Delta\widetilde{C} = \widetilde{C}_n - \widetilde{C}_f$ is the enhanced solubility at grain contact sites, expressed as the local mean undersaturation of the grain boundary solution phase with respect to the adjacent stressed solid and where $I_s = \alpha k_+ \Omega$.

The enhancement of solid solubility at stressed grain contact sites relative to the solute concentration in the local grain boundary fluid phase, and relative to the solubility at the unstressed pore walls, can now be expressed using the standard relation for the chemical potential of dissolved solid in a dilute (ideal) solution (e.g. Chang 2000). Applying this relationship for a grain boundary (source) element transmitting a local mean normal stress $\widetilde{\sigma}_n$, the normal component of the chemical potential of the solid at the element boundary (Lehner 1990; Van Noort & Spiers 2009) can be written as $\widetilde{\mu}_n = \mu_0 + RT\ln(\widetilde{C}_n/C_0)$ where μ_0 is the solute potential at the reference concentration C_0. Similarly, the potential of the solid at free pore wall sites (i.e. the potential of the solute in local equilibrium with the more or less unstressed solid at pore wall sites) can be written as $\mu_{pw} = \mu_0 + RT\ln(C_{pw}/C_0)$ where C_{pw} is the solubility of the solid at such pore wall (sink) sites. The chemical potential difference between source and sink sites $\Delta\widetilde{\mu}_n$ can therefore be written $\Delta\widetilde{\mu}_n = \widetilde{\mu}_n - \mu_{pw} = RT\ln(\widetilde{C}_n/C_{pw})$. However, in the case of dissolution-controlled pressure solution, that is $\Delta\widetilde{\mu}_n = \Delta\widetilde{\mu}_s$, the potential drop is driving the grain boundary dissolution reaction and $\Delta\widetilde{\mu}_d \approx \Delta\widetilde{\mu}_p \approx 0$. This means that there is negligible potential difference between the solute in the grain boundary fluid ($\widetilde{\mu}_f$) and the solid phase at the pore walls, so that $\widetilde{\mu}_f \approx \mu_{pw}$ and hence $\widetilde{C}_f \approx C_{pw}$. On this basis, we can write

$$\Delta\widetilde{\mu}_n = \widetilde{\mu}_n - \widetilde{\mu}_f = RT\ln\frac{\widetilde{C}_n}{\widetilde{C}_f} = RT\ln\frac{\widetilde{C}_f + \Delta\widetilde{C}}{\widetilde{C}_f}$$
$$= RT\ln\left(1 + \frac{\Delta\widetilde{C}}{\widetilde{C}_f}\right)$$

or

$$\frac{\Delta\widetilde{C}}{\widetilde{C}_f} = \left[\exp\left(\frac{\Delta\widetilde{\mu}_n}{RT}\right) - 1\right] \approx \frac{\Delta\widetilde{C}}{C_{pw}}.$$

The velocity of dissolution at local grain boundary source sites is hence given as

$$\widetilde{V}_c = I_s\left[\exp\left(\frac{\Delta\widetilde{\mu}_n}{RT}\right) - 1\right].$$

Since we assume that dissolving grain-to-grain contacts remain flat, this dissolution velocity must be uniform over each grain contact area so that $\Delta\widetilde{\mu}_n$ and hence $\widetilde{\mu}_n$ and the normal stress $\widetilde{\sigma}_n$ must also be uniform across the grain contact area. Accordingly, we can write the average potential drop across grain contacts as $\Delta\mu_n = \Delta\widetilde{\mu}_n$ and the average contact stress as $\sigma_n = \widetilde{\sigma}_n$. The uniform velocity of dissolving grain contact surfaces V_c, the uniform average velocity measured at the grain contact scale, can therefore be written as

$$V_c = \widetilde{V}_c = I_s\left[\exp\left(\frac{\Delta\mu_n}{RT}\right) - 1\right]$$

which, upon insertion of Equation (5), yields

$$V_c = I_s\left[\exp\left(\frac{\sigma_n^e \Omega}{RT}\frac{Z}{F}\frac{q}{q-2\phi}\right) - 1\right]. \qquad (6)$$

With reference to Figure 2, the shortening strain rate in any principal direction normal to a grain contact can now be obtained using the kinematic relation $\dot{\varepsilon}_x \approx V_s/(d/2)$, so that the (isotropic) 3D volumetric strain rate response to applied hydrostatic stress can be written as

$$\dot{\varepsilon}_{3D} = 3\dot{\varepsilon}_x = \frac{6V_c}{d}. \qquad (7)$$

Downloaded from http://sp.lyellcollection.org/ at Universiteitsbibliotheek Utrecht on October 27, 2015

Combining this with Equation (6) gives our rate expression for compaction by dissolution-controlled pressure solution as

$$\dot{\varepsilon}_s = \frac{A_s}{d} I_s \left[\exp\left(\frac{\sigma_n^e \Omega}{RT} \frac{Z}{F} \frac{q}{q-2\phi} \right) - 1 \right] \quad (8)\ [\text{Model S}]$$

where $A_s = 6$ for 3D isotropic compaction. For pure 1D compaction, the factor 3 in Equation (7) disappears so that $A_s = 2$. This implies that for 1D compaction of a real, imperfectly packed, granular aggregate, in which the stress state will be intermediate between uniaxial and hydrostatic, A_s will take an intermediate value of 4 ± 2. At low stresses, the $[\exp(x) - 1]$ term can of course be approximated by x, leading to a linear dependence of strain rate on applied effective stress σ_n^e.

For completeness, we note that an identical result to Equation (8) is obtained by assuming that all of the mechanical work $\dot{W} = \sigma_n^e \dot{\varepsilon}_s$ (J m^{-3} s^{-1}) done per second in compacting the aggregate by pressure solution is dissipated by the dissolution step. The dissipation or energy release rate by dissolution per grain contact is given by $\dot{\Delta}_c = \Delta\mu_n V_c a_c / \Omega$ (cf. Lehner 1990) and hence per unit volume of aggregate by $\dot{\Delta}_s = \dot{\Delta}_c[(1/d_s^3)(2/Z)]$ where the term in square brackets is the number of grain contacts per unit volume. Combining these relations for $\dot{\Delta}_s$ with the approximation $d_s \approx d$ with Equation (3) for a_c and with Equation (5) for $\Delta\mu_n$, and setting $\dot{W} = \sigma_n^e \dot{\varepsilon}_s = \dot{\Delta}_s$, leads to Equation (8).

Precipitation-controlled compaction creep. When precipitation is rate controlling, $\Delta\mu_n \approx \Delta\mu_p$. Neglecting small changes in the mass of solid stored in the (supersaturated) pore fluid during precipitation-controlled compaction, mass conservation requires that the amount of material that precipitates on pore walls also dissolves from grain contacts. This means that $V_{pw} A_{pw} \approx V_c A_c$, where V_{pw} is the pore wall growth velocity controlled by the precipitation rate, A_{pw} is the pore wall area per grain, V_c is the contact dissolution velocity and A_c is the total contact area per grain. Recalling that $F = \pi$ for spherical grains, then by taking the total grain contact area per grain as $A_c = Z a_c$ the total pore wall area per grain can be written as $A_{pw} = Fd^2 - A_c$. Rearranging our expression for mass conservation yields $V_c = V_{pw} A_{pw} / A_c = V_{pw}[(Fd^2 - Za_c)/Za_c]$. Use of Equation (3) now leads to an expression for the precipitation-controlled velocity of dissolution at grain contacts:

$$V_c = V_{pw} \frac{Fd^2 - Fd^2 f(\phi)}{Fd^2 f(\phi)} = V_{pw} \frac{1 - f(\phi)}{f(\phi)}.$$

Assuming that the precipitation reaction on pore walls obeys a growth velocity law of the same type as the dissolution rate law assumed for grain contacts, but written without any influence of grain boundary structure on precipitation rate (i.e. with $\alpha = 1$), then the precipitation velocity V_{pw} can be expressed as $V_{pw} = k_+ \Omega(\Delta C_{pw}/C_{pw})$ where ΔC_{pw} is the solute supersaturation in the pore fluid with respect to the pore walls, or alternatively as $V_{pw} = I_{pw}(\Delta C_{pw}/C_{pw})$ (where $I_{pw} = k_+ \Omega$). At the same time, for precipitation control we know that $\Delta\widetilde{\mu}_s \approx \Delta\widetilde{\mu}_d \approx 0$ and that $\Delta\mu_s \approx \Delta\mu_d \approx 0$, so there is negligible potential difference between the solid within the grain boundary source elements and the solute within either the grain boundary fluid or the open pores (see also De Meer & Spiers 1997). Consistent with the assumption that the dissolving grain contacts remain flat, and with the mechanics of uniform contact loading, we further assume that the enhanced solubility of the solid within individual grain boundary elements ($\widetilde{C_n}$) is uniform across the contacts, so that the average enhanced solubility at the contact scale can be written as $C_n = \widetilde{C_n}$. The average potential of the solid at grain contacts can accordingly be written as $\mu_n = \widetilde{\mu_n}$ and the average normal stress as $\sigma_n = \widetilde{\sigma_n}$, whereby both $\widetilde{\mu_n}$ and $\widetilde{\sigma_n}$, like $\widetilde{C_n}$, are uniform across the contacts. This means that $\Delta C_{pw} \approx C_n - C_{pw}$, so that $V_{pw} = I_{pw}[C_n/C_{pw} - 1]$ which, applying $\mu = \mu_0 + RT \ln(C/C_0)$ for μ_n and μ_{pw}, yields $V_{pw} = I_{pw}[\exp(\Delta\mu_p/RT) - 1]$ as the precipitation velocity on pore walls, where $\Delta\mu_p = \Delta\mu_n = \mu_n - \mu_{pw}$. Applying Equation (5) now yields $V_{pw} = I_{pw}\{\exp[(\sigma_n^e \Omega/RT)(Z/F)q/(q-2\phi)] - 1\}$ which, together with $V_c = V_{pw}[(1 - f(\phi))/f(\phi)]$ and Equations (4) and (7) leads to the precipitation-controlled compaction rate:

$$\dot{\varepsilon}_p = \frac{A_p}{d} I_{pw} \left[\exp\left(\frac{\sigma_n^e \Omega}{RT} \frac{Z}{Ff(\phi)} \right) - 1 \right] \frac{2\phi}{(q-2\phi)} \quad (9)\ [\text{Model P}]$$

where $A_p = 6$ for isotropic compaction, while for 1D compaction of a granular aggregate $A_p = 4 \pm 2$. As for dissolution control, the $[\exp(x) - 1]$ term can be approximated by x when applied stresses are low, leading to a linear dependence of strain rate on applied effective stress σ_n^e.

Also in this case, an identical result to Equation (9) can be obtained by assuming that all of the mechanical work $\dot{W} = \sigma_n^e \dot{\varepsilon}_p$ done per unit volume of aggregate per second is dissipated by the rate-controlling process, that is, precipitation. This dissipation is given as $\dot{\Delta}_{pw} = \Delta\mu_n V_{pw} A_{pw}/\Omega$ per grain and as $\dot{\Delta}_p = \dot{\Delta}_{pw}/d_s{}^3 \approx \dot{\Delta}_{pw}/d^3$ per unit volume. Combining these relations for $\dot{\Delta}_p$ with the

Downloaded from http://sp.lyellcollection.org/ at Universiteitsbibliotheek Utrecht on October 27, 2015

approximation $d_s \approx d$ with $A_{pw} \approx Fd^2 - A_c$, with Equation (3) for a_c, and with Equation (5) for $\Delta\mu_n$, and putting $\dot{W} = \sigma_n^e \dot{\varepsilon}_p = \dot{\Delta}_p$ also leads to Equation (9).

Diffusion-controlled compaction creep. In the case of diffusion-controlled creep, all of the potential drop $\Delta\widetilde{\mu}_n$ between local grain boundary source sites and pore walls is consumed in driving grain boundary diffusion, as is the average potential drop $\Delta\mu_n$ between the entire grain contact and pore walls, so that $\Delta\mu_n = \Delta\mu_d$. Again, this is equivalent to stating that the mechanical work done in causing compaction is fully dissipated in driving grain boundary diffusion (Lehner 1990; Spiers & Schutjens 1990). Many authors have derived models for creep by diffusion-controlled pressure solution using a variety of approaches. However, all make essentially equivalent assumptions and approximations. The result obtained for the strain rate was elegantly given by Rutter (Rutter 1976; see also Lehner 1995) as

$$\dot{\varepsilon} = \frac{32\Omega D C_0 S}{RT\rho}\frac{\sigma_n}{d^3} \tag{10}$$

which is the classical result for the process, where D ($m^2\ s^{-1}$) is the diffusion coefficient, C_0 is the solubility of the solid (measured here in kg mol^{-1}), ρ is the density of the solid and S is the fluid film thickness. Here we will derive models for compaction creep by diffusion-controlled pressure solution using several different approaches, explicitly making or avoiding the assumptions and approximations employed previously.

In the simplest approach, the average potential difference between the solid within grain contacts and at pore walls can be written as $\Delta\mu_n = \Delta\mu_d = (\sigma_n - P_f)\Omega \approx (Z/F)(\sigma_n^e\Omega)q/(q-2\phi)$ (see Equations (1)–(5)). The equivalent concentration difference driving diffusion is, of course, the mean solubility difference between grain contacts and pore walls. Using the standard relation $\mu = \mu_0 + RT\ \ln(C/C_0)$, this yields $\Delta C_d/C_{pw} \approx \Delta C_d/C_0 = \exp(\Delta\mu_d/RT) - 1$. With reference to Figure 3, the mean potential gradient driving diffusion out of the contacts can now be approximated as $\partial\mu_d/\partial r \approx \Delta\mu_d/(\beta a)$ where a is the radius of the contact periphery and β is a geometric factor of the order 0.5 (noting that the average diffusion distance will be about half of the radius of the contact periphery a). The corresponding mean concentration gradient can be written as $\partial C/\partial r \approx \Delta C_d/(\beta a)$ or $\partial C/\partial r \approx C_0[\exp(\Delta\mu_d/RT) - 1]/(\beta a)$. The resulting mean radial diffusion flux J is now given using Fick's first law as $J = -D(\partial C/\partial r)$ or $J = -DC_0[\exp(\Delta\mu_d/RT) - 1]/(\beta r)$, in which

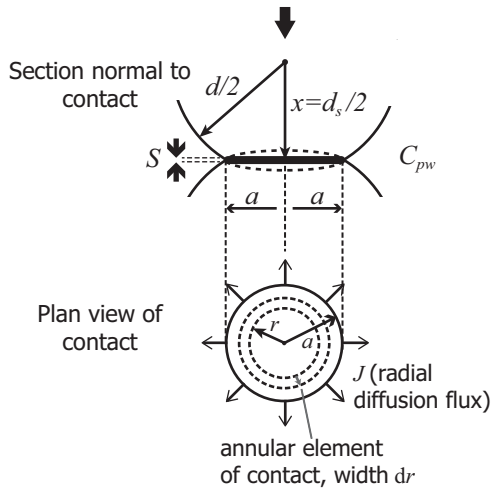

Fig. 3. Grain contact geometry used for analysing diffusion-controlled pressure solution. Symbols defined in Table 1.

D ($m^2\ s^{-1}$) is the diffusion coefficient and C_0 is the solubility of solute in the grain boundary fluid under hydrostatic conditions (mol m^{-3}). This flux passes through a circular window at the grain contact periphery (radius a) of area $2\pi aS$, where S is the average thickness of fluid in the grain boundary (Fig. 3). The number of moles of dissolved solid diffusing out of the grain contact periphery is therefore $2\pi aSJ$, which corresponds to a volume flux of $2\pi aSJ\Omega$. Mass balance then requires material to dissolve from the grain contact with a velocity

$$V_c = \frac{2\pi D C_0 S\Omega}{\beta a_c}\left[\exp\left(\frac{\Delta\mu_d}{RT}\right) - 1\right] \tag{11}$$

which with use of Equations (3) and (4) plus (5) and (7) yields:

$$\dot{\varepsilon}_{d1} = \frac{2\pi A_c D C_s S Z}{\beta F d^3}\left[\exp\left(\frac{\sigma_n^e\Omega}{RT}\frac{Z}{F}\frac{q}{q-2\phi}\right) - 1\right] \times \left(\frac{q}{q-2\phi}\right) \tag{12}$$

[Model D1]

where $C_s = C_0\Omega$ ($m^3\ m^{-3}$). When $(\sigma_n^e\Omega/RT)(Z/F)\ q/(q-2\phi)$ is small this can be approximated as

$$\dot{\varepsilon}_{d2} = \frac{2\pi A_c D C_s S Z^2}{\beta F^2 d^3}\frac{\sigma_n^e\Omega}{RT}\left(\frac{q}{q-2\phi}\right)^2 \tag{13}$$

[Model D2]

Downloaded from http://sp.lyellcollection.org/ at Universiteitsbibliotheek Utrecht on October 27, 2015

Table 1. *Symbols used in text*

Symbol	Definition	Unit
~	Embellishment indicating that the quantity below it is defined on a local scale	
d, p, s	Subscripts indicating diffusion, precipitation or dissolution control, respectively	
α	Factor allowing for the influence of grain boundary structure on grain boundary dissolution rate	–
a	Grain contact periphery radius	m
$A_{d,p,s}$	Geometric factor depending on packing plus deformation geometry (1D v. 3D compaction)	–
A_{pw}	Pore wall area per grain	m^2
A_c	Grain contact area per grain	m^2
a_c	Area of an individual grain contact	m^2
β	Geometric factor accounting for diffusion distance	–
C_0	Solubility in the unstressed (hydrostatic) case	mol m^{-3}
C	Solubility of stressed material	mol m^{-3}
C_f	Concentration of dissolved solid in grain boundary fluid	mol m^{-3}
ΔC	Absolute enhancement in the solubility of the solid at stressed grain contacts	mol m^{-3}
C_s	Local mean concentration of dissolved solid in grain boundary fluid	mol m^{-3}
C_{pw}	Solubility of the solid at pore wall (sink) sites	mol m^{-3}
C_s	Average solubility of solute in the grain boundary fluid	m^3 m^{-3}
ΔC_{pw}	Solute supersaturation in the pore fluid with respect to the pore walls	mol m^{-3}
C_n	Enhanced solubility of the solid	mol m^{-3}
d_s	Truncated diametral grain spacing	m
d_p	Grain diameter measured at pore wall	m
d	Mean grain diameter	m
D	Grain boundary diffusion coefficient	m^2 s^{-1}
$\dot{\Delta}_c$	Dissipation or energy release rate by dissolution per grain contact	J s^{-1}
$\dot{\Delta}_{d,p,s}$	Dissipation per unit volume of aggregate for dissolution-controlled pressure solution	J m^{-3} s^{-1}
$\dot{\Delta}_{pw}$	Dissipation per grain contact by precipitation-controlled pressure solution	J s^{-1}
$d\dot{\Delta}_r$	Incremental dissipation rate	J s^{-1}
$\dot{\Delta}_t$	Total energy dissipation due to solute diffusion out of contact zone	J m^{-3} s^{-1}
$\dot{\varepsilon}$	Strain rate	s^{-1}
ϕ	Porosity of grain aggregate	–
ϕ_0	Maximum porosity of a regular pack of spherical grains at the point where grains just touch	–
ϕ_{0C}	Porosity at initiation of creep in uniaxial compaction experiments (Pluymakers *et al.* 2014)	–
F	Grain shape factor (π for spherical grains)	–
h	Geometric factor, in current models equal to 1	–
I_s	Dissolution rate constant ($\alpha k_+ \Omega$)	m s^{-1}
I_{pw}	Precipitation rate constant ($k_+ \Omega$)	m s^{-1}
J	Pointwise solute flux in the grain contact fluid	mol m^{-2} s^{-1}
k_+	Geochemical dissolution rate constant for the unstressed solid	mol m^{-2} s^{-1}
μ_0	Solute chemical potential at a reference concentration (C_0) in solution	J
μ_f	Chemical potential of the solute in grain boundary fluid	J
μ_n	Chemical potential	J
μ_{pw}	Chemical potential of the solid at the pore wall	J
$\Delta\mu_{d,p,s}$	Chemical potential drop associated with d-, p- or s-controlled pressure solution	J
$\Delta\mu_n$	Drop in normal component of chemical potential	J
P_f	Fluid pressure acting on the free pore walls	MPa
P	Total applied hydrostatic stress	MPa
q	Geometric term equal to $2\phi_0$	–
ρ	Solid density	kg m^{-3}
R	Gas constant	J mol^{-1} K^{-1}
r	Radial coordinate within grain contacts	m
σ_n^e	Effective normal stress imposed on the aggregate	MPa

(*Continued*)

Downloaded from http://sp.lyellcollection.org/ at Universiteitsbibliotheek Utrecht on October 27, 2015

Table 1. *Continued.*

Symbol	Definition	Unit
σ_n	Average normal stress transmitted across grain contacts	MPa
S	Mean fluid film thickness	m
T	Absolute temperature	K
V_c	Uniform velocity of dissolving grain contact surfaces	ms^{-1}
V_{pw}	Pore wall growth velocity	ms^{-1}
$\dot{W}$	Mechanical work rate ($\sigma_n^e \dot{\varepsilon}_s$)	$Jm^{-3}\,s^{-1}$
Z	Grain coordination number	–
Ω	Molar volume of solid phase	$m^3\,mol^{-1}$

since $[\exp(x) - 1] \rightarrow x$ for small x. For appropriate values of the constants β, Z and F, this is exactly equivalent to the result obtained for diffusion control by Rutter (1976) and Lehner (1990).

A more rigorous approach, following that adopted by Lehner (1990), Spiers & Schutjens (1990) and Schutjens & Spiers (1999) and ultimately equivalent to that adopted by Rutter (1976), involves equating the mechanical work rate $\dot{W}$ ($J\,m^{-3}\,s^{-1}$) to the rate of dissipation by grain boundary diffusion $\dot{\Delta}_d$. We pursue this here, first including and then avoiding the approximations used in previous treatments, to arrive at fully rigorous results. We prefer this to Rutter's approach as it avoids his assumption of static stress equilibrium at grain contacts which, for diffusion control, requires a static parabolic stress distribution (see discussion by Lehner 1995). We start with reference to Figure 3, noting that the approach velocity of the two grain centres is $2V_c$ ($m\,s^{-1}$) where V_c is the uniform contact dissolution velocity. For a circular region of an individual grain contact of radius r (m), and for mean grain boundary fluid film thickness S (see Fig. 3), mass conservation requires that at steady state the total outward flux (mol s^{-1}) equals the total material input due to dissolution (mol s^{-1}), so that

$$J(r) \cdot 2\pi r S = 2V_c \pi r^2/\Omega. \tag{14}$$

Combining this with Fick's law gives:

$$J(r) = \frac{V_c r}{S\Omega} = -D\frac{\partial C}{\partial r}. \tag{15}$$

Differentiating $\mu = \mu_0 + RT\ln(C/C_0)$ (e.g. Chang 2000) with respect to C now yields $\partial\mu/\partial C = RT/C$ which, combined with Equation (15), leads to:

$$J(r) = \frac{V_c r}{S\Omega} = -D\frac{\partial C}{\partial \mu}\frac{\partial \mu}{\partial r} = -\frac{DC(r)}{RT}\frac{\partial \mu}{\partial r} \tag{16}$$

for the diffusion flux at any point in the grain boundary fluid. This flux produces an energy dissipation per unit volume of magnitude $\dot{\Delta}_r = -J(r)(\partial\mu/\partial r)$ ($J\,m^{-3}\,s^{-1}$, Lehner 1990). The dissipation increment $d\dot{\Delta}_r$ ($J\,s^{-1}$) occurring in a radius interval dr of the contact zone (i.e. at $r \leq a$; see Fig. 3) can hence be written as:

$$d\dot{\Delta}_r = -J(r)\frac{\partial \mu}{\partial r} S\, 2\pi\, r\, dr. \tag{17}$$

Substituting for $\partial\mu/\partial r$ from Equation (16) and integrating Equation (17) over the entire grain contact (radius a) now gives the total dissipation $\dot{\Delta}_t$ due to solute diffusion out of the contact zone as:

$$\dot{\Delta}_t = \frac{2\pi SRT}{D}\int_0^a \frac{J(r)^2 r}{C(r)}\, dr$$

$$= \frac{2\pi RTV_c{}^2}{DS\Omega^2}\int_0^a \frac{r^3}{C(r)}\, dr. \tag{18}$$

All authors (Lehner 1990; Spiers & Schutjens 1990; Schutjens & Spiers 1999) now essentially follow Rutter (Rutter 1976) in assuming that $C(r)$ can be taken as constant and approximately equal to the solute concentration in the pores, so that $C(r) \approx C_{pw} \approx C_0$, which is valid for low grain contact stresses, that is, small departures from C_0. The integral in Equation (18) can then be evaluated simply as:

$$\dot{\Delta}_t = \frac{2\pi RTV_c{}^2}{DS\Omega^2 C_{pw}}\int_0^a r^3\, \partial r = \frac{\pi RTV_c{}^2}{2DS\Omega^2 C_{pw}} a^4. \tag{19}$$

Our assumption that all work ($\dot{W}$) done by the stress applied to the grain contact is dissipated through diffusion-controlled pressure solution then allows us to write:

$$\dot{W} = 2\sigma_n V_c \pi a^2 = \dot{\Delta}_t \tag{20}$$

Downloaded from http://sp.lyellcollection.org/ at Universiteitsbibliotheek Utrecht on October 27, 2015

which, using Equation (19), yields:

$$V_c = \frac{4DC_{pw}S\Omega^2}{RT}\frac{\sigma_n}{a^2} \quad (21)$$

for the velocity of contact dissolution. Noting that the grain contact radius a is related to its area a_c via $a_c = \pi a^2$, and using Equations (3) and (4), we can subsequently write:

$$a = \sqrt{\frac{F}{Z\pi}\frac{q-2\phi}{q}d^2}. \quad (22)$$

Combining this with Equations (21) and (7) leads to our final expression for diffusion-controlled pressure solution obtained using the energy dissipation balance approach plus the assumption $C(r) = C_{pw} = C_0$ in Equation (18):

$$\dot{\varepsilon}_{d3} = \frac{4\pi A_d Z}{F}\frac{DC_sS}{d^3}\frac{\sigma_n^e\Omega}{RT}\frac{Z}{F}\left(\frac{q}{q-2\phi}\right)^2 \quad (23)\ [\text{Model D3}]$$

where A_d is 6 for isotropic compaction and lies in the range 4 ± 2 for 1D strain, as in the case for dissolution- and precipitation-controlled creep. Note that $C_0\Omega$ is again replaced by C_s, where C_s is now in $m^3\,m^{-3}$. Note also that Equation (23) is exactly equivalent to Equation (13) for $\beta = 0.5$. It is also identical to the result obtained using Rutter's approach, which yields a similar expression but with different geometric constants.

The above are consistent with models for diffusion-controlled pressure solution derived by previous authors (Rutter 1976; Lehner 1990; Schutjens & Spiers 1999; Spiers *et al.* 2004). However, a fully rigorous approach needs to take the change in solubility $C(r)$ over the grain contact into account in Equation (18). This can be done by rewriting Equation (15) to obtain $\partial C = -V_c r/(S\Omega D)\partial r$, or $C(r) = -V_c/(S\Omega D)\int r\,dr$. Solving this integral and noting that $C = C_{pw}$ when $r = a$ yields

$$C(r) = C_{pw} + \frac{V_c}{2S\Omega D}(a^2 - r^2). \quad (24)$$

Inserting this into the integral in Equation (18) and making use of the Lambert W function, which gives the solution for X in $Y = Xe^X$ as $X = W(Y)$, then the expression obtained via Equations (18–20) for the contact dissolution velocity V_c is

$$V_c = \frac{2}{a^2}DC_sS\frac{B - W(Be^B)}{W(Be^B)} \quad (25)$$

in which $B = -[(\sigma_n\Omega/RT) + 1] = -[(Z/F)\,q/(q-2\phi)(\sigma_n^e\Omega/RT) + 1]$. Use of Equations (7) and (22) then leads to the following, fully rigorous expression for the diffusion-controlled compaction strain rate, namely:

$$\dot{\varepsilon}_{d4} = \frac{2\pi A_d Z}{Fd^3}DC_sS\frac{B - W(Be^B)}{W(Be^B)}\frac{q}{q-2\phi} \quad (26)\ [\text{Model D4}]$$

with A_d is 4 ± 2 for 1D strain.

Model implementation and comparison with experimental data

The models derived above can be applied to any material that deforms by solution transfer from stressed, fluid-filled grain contacts to pore walls. We now implement our models to describe dissolution-controlled (Equation (8)), precipitation-controlled (Equation (9)) and diffusion-controlled pressure solution (models D1, 2, 3 and 4 in Equations (12), (13), (23) and (26), respectively) of granular anhydrite, by inserting parameter values appropriate for that mineral. Our aim is to predict the evolution of compaction creep rate with progressively decreasing (normalized) porosity (ϕ/ϕ_0) for anhydrite fault gouge, and to compare the predictions obtained for the different rate-controlling processes. Recall here that ϕ_0 in our models is the porosity at which grain contact areas are infinitesimally small, that is, the aggregate porosity at zero creep strain. We go on to compare the various models with the experimental data on compaction of simulated anhydrite fault gouge obtained by Pluymakers *et al.* (2014) in their experiments performed at 80 °C and 5–12 MPa effective stress (see Fig. 1), using the experimentally measured values of ϕ/ϕ_{0C} to cast the experimental data in the form of strain rate v. equivalent ϕ/ϕ_0 data (see Fig. 1). This recasting operation was carried out on the basis of the fact that that the porosity of our uncompacted anhydrite starting powders lay between 46% and 50% (i.e. close to the value of $\phi_0 = 48.5\%$, characterizing our model grain pack), then simply multiplying ϕ/ϕ_{0C} by $\phi_{0C}/(0.485)$. The resulting comparison of experiment v. theory enables us to simultaneously test the applicability of the models derived above, and to test the hypothesis advanced by Pluymakers *et al.* that compaction of anhydrite in the fine-grained creep regime of Figure 1 involved diffusion-controlled pressure solution (Fig. 1). The values used for the parameters appearing in our model equations are given in Table 2. Note that in the case of diffusion control, we used values for the grain boundary diffusion product DS that fall in the same range as reported for pressure solution in other ionic compounds, such as NaCl and calcite (e.g. Spiers & Schutjens

Downloaded from http://sp.lyellcollection.org/ at Universiteitsbibliotheek Utrecht on October 27, 2015

1990; Spiers *et al.* 2004; De Meer *et al.* 2005; Zhang and Spiers 2005; Zhang *et al.* 2010; Koelemeijer *et al.* 2012).

Our calculations on creep rate v. ϕ/ϕ_0, made using the full set of models, are compared in Figure 4. This shows that diffusion-controlled pressure solution is predicted to be 1–3 orders of magnitude slower than either dissolution-controlled (S) or precipitation-controlled (P) pressure solution in anhydrite under the conditions of the experiments reported by Pluymakers *et al.* (2014) (Fig. 4), regardless of the specific diffusion model applied (D1–D4) and despite the range in the values taken for the grain boundary diffusion product *DS*. Note here that the available data on anhydrite dissolution kinetics determined by Blount & Dickson (1969) likely underestimate the true rates of dissolution and precipitation. This is because those reactions are so fast they are difficult to measure independently of diffusion effects. The implication is that pressure solution in anhydrite will generally be diffusion controlled for a wide range of grain sizes, effective stresses and temperatures as well as those shown in Figure 4.

Comparison of the diffusion-controlled pressure solution models D1 and D4 with each other in Figure 4a shows they are almost indistinguishable for each of the chosen values of the parameter *DS*. Regarding the linearized models for diffusion-controlled creep, that is, models D2 and D3 plotted in Figure 4b, these are equivalent to each other and so give identical results despite the difference in derivation. They yield lower creep rates than either D1 or D4 at normalized porosities $\phi/\phi_0 \geq 0.95$, that is, for small grain-to-grain contact areas and high contact stresses. At $\phi/\phi_0 \leq 0.9$ however, all four diffusion-controlled models yield strain rate predictions within a factor of 2 for any given value of *DS* and at $\phi/\phi_0 \leq 0.6$ the four models are indistinguishable for practical purposes.

Figure 5 compares the experimental data for the wet fine-grained samples of Pluymakers *et al.* (2014) with the predictions of the diffusion-controlled rate models (D1–D4) applied for the same *DS* values used in Figure 4. This shows that the experimental strain rates match the diffusion-controlled rates within one order of magnitude, although the sensitivity of compaction strain rate to changing porosity (expressed as ϕ/ϕ_0) is much higher for the experimental samples than predicted by the diffusion-controlled models. At the same time, the experimentally determined strain rates are 100–1000 times lower than the rates predicted for dissolution- and precipitation-controlled pressure solution (compare Figs 4 & 5). The similarity between the diffusion-controlled pressure solution models and the experimental strain rates strongly suggests that our diffusion-controlled pressure solution models offer a rough estimate and explanation of the compaction creep rates measured for the fine-grained anhydrite fault gouges, despite differences in assumed v. real grain shape, packing and grain size distribution. This supports the inference by Pluymakers *et al.* (2014) that the behaviour of fine-grained anhydrite is dominated by pressure solution and specifically by diffusion-controlled pressure solution. The order of magnitude agreement between the creep rates predicted by our diffusion-controlled models and the experimental data also imply that the models provide a basis for

Table 2. *Values of the parameters used in applying the present pressure solution models*

Symbol	Definition	Value/range	Source and additional information (where applicable)
α	Geometric factor	0.9	Van Noort & Spiers (2009)
A	Geometric constant	4	Average value for simple cubic pack of grains
C_s	Anhydrite solubility ($m^3\ m^{-3}$)	4.7×10^{-4}	Blount & Dickson (1969)
DS	Product equal to diffusion coefficient D times mean grain boundary fluid thickness S ($m^3\ s^{-1}$)	10^{-19} to 10^{-20}	Range determined for diffusion-controlled pressure solution in other ionic compounds such as NaCl and calcite (e.g. De Meer *et al.* 2005; Koelemeijer *et al.* 2012; Zhang *et al.* 2010)
F	Grain shape factor	π	Value for simple cubic pack of grains
k^+	Rate constant for dissolution/precipitation of anhydrite ($m\ s^{-1}$)	5.11×10^{-7} $T^{1.186902}$	Minimum values determined by Bildstein *et al.* (2001)
R	Gas constant ($J\ mol^{-1}\ K^{-1}$)	8.314	For example Chang (2000)
Z	Coordination number	6	Value for simple cubic pack of grains
Ω	Molar volume of anhydrite $CaSO_4$ ($m^3\ mol^{-1}$)	4.6×10^{-5}	Hummel *et al.* (2002); Thoenen & Kulik (2003)

Downloaded from http://sp.lyellcollection.org/ at Universiteitsbibliotheek Utrecht on October 27, 2015

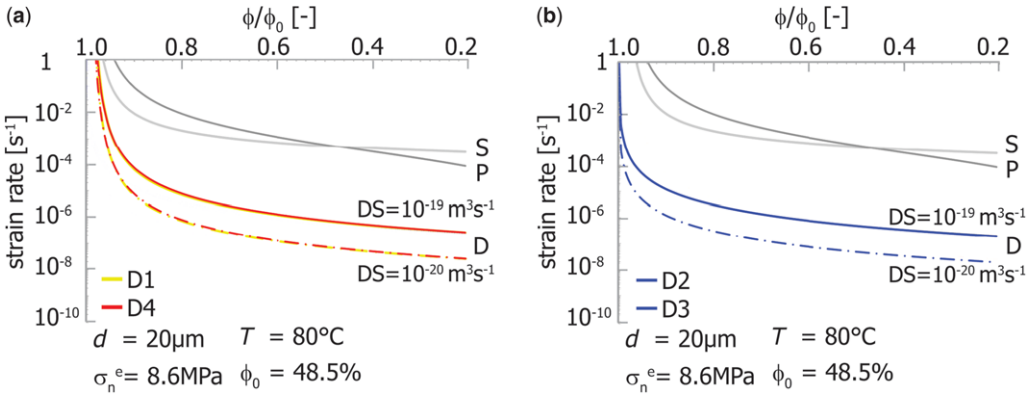

Fig. 4. Comparison of predictions of all pressure solution models derived here, for all rate-controlling steps considered (dissolution-controlled Model S, precipitation-controlled Model P, diffusion-controlled Model D1, D2, D3 and D4; see text for details). The temperature T, applied effective stress σ_n^e, starting porosity ϕ_0 and grain size d used for these calculations are chosen to be representative of the compaction experiments on wet anhydrite reported by Pluymakers *et al.* (2014). The model parameter values used are given in Table 2. Note that the diffusion-controlled models D1 to D4 are plotted for *DS* values of 10^{-19} m^3 s^{-1} (top) and for 10^{-20} m^3 s^{-1} (bottom). (**a**) Model predictions for S and P v. D1 and D4. (**b**) Model predictions for S and P v. D2 = D3.

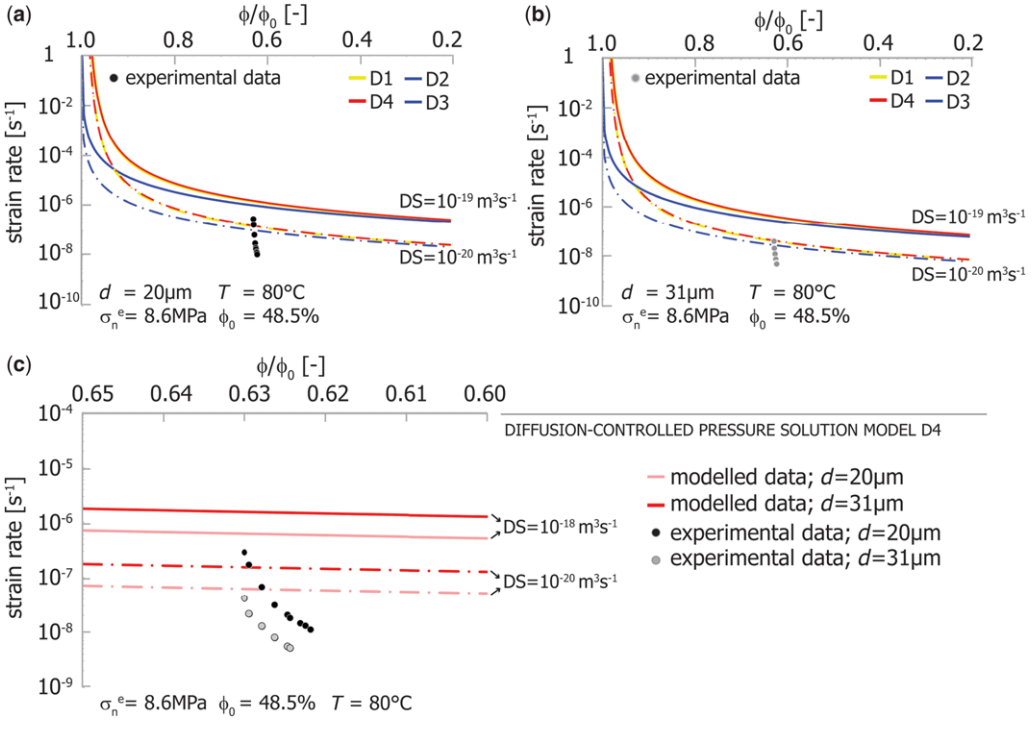

Fig. 5 Prediction of compaction strain rate v. normalized porosity (ϕ/ϕ_0) for the different diffusion-controlled pressure solution models derived here (D1–D4) plus comparison with the experimental data reported by Pluymakers *et al.* (2014) (errors in log strain rate fall (just) within the symbol size). *DS*-values are 10^{-19}–10^{-20} m^3 s^{-1}. (**a**) Grain size $d = 20$ μm; (**b**) grain size $d = 31$ μm; and (**c**) both grain sizes plus total range covered by the predictions of model D4 only. Symbols as in Figure 4 and Table 2.

Downloaded from http://sp.lyellcollection.org/ at Universiteitsbibliotheek Utrecht on October 27, 2015

roughly predicting rates of pressure solution in anhydrite gouges under natural conditions, that is, for extrapolating to nature.

As indicated above, however, a clear discrepancy exists between the experimental results and models D1–D4 as plotted in Figure 5, in that the experimental strain rates (1) are initially too rapid if extrapolated to higher values of ϕ/ϕ_0 and (2) decelerate more rapidly than the models predict at the sample porosities investigated (*c.* 30%). In an attempt to explain this, we note that all of our models are based on an aggregate of cubic packed spherical grains whereas, in reality, the grains are characterized by tabular or blocky shapes and, more importantly, have a rough irregular surface (see Pluymakers *et al.* 2014). These factors will strongly influence the evolution of grain contact area, contact stresses and transport path lengths during the progress of compaction. For example, irregularities in the grain surface morphology may lead to high stresses at contact points, which will dissolve rapidly until the grain contact is smoother. This type of behaviour may explain the initially rapid deceleration of strain rate with increasing strain seen in the experiments (see Fig. 5a–c). Such behaviour is also consistent with the observation that, towards the end of the experiments, the measured strain rates follow the same trend as the lower bound of the modelled strain rates (Fig. 5c), suggesting that contact roughness and irregularities are being progressively removed and the model microstructure more closely approached. Seen in this context, the fact that the grain size dependence on strain rate seen in the experimental data is consistent with the $1/d^3$ relationship predicted by the diffusion-controlled models is perhaps surprising. On the other hand the dimensions of the grain surface irregularities, seen in the microstructure of the granular anhydrite used in the experiments, do scale roughly with grain size (Pluymakers *et al.* 2014). Purely plastic deformation or else brittle crushing of grain surface asperities are difficult to eliminate as alternative mechanisms of grain contact smoothening, as opposed to dissolution. These mechanisms do seem unlikely however, given that Pluymakers *et al.* (2014) reported negligible creep deformation in dry-tested samples.

Implications for fault healing and CO_2 storage

Having shown that our diffusion-controlled models seem capable of approximating experimental strain rates in simulated anhydrite fault gouge tested at temperature, stress and fluid pressure conditions that are at least of the same order as expected in the upper crust, we now apply our models to evaluate healing and sealing of (reactivated) faults in anhydrite rocks in nature (the stable phase of $CaSO_4$ at depths greater than 2–2.5 km). We assume that the (re)activated cores of the faults considered are filled with mainly fine-grained anhydrite fault gouge and are fully wetted by $CaSO_4$-saturated aqueous fluid. We first apply our models to estimate sealing times for anhydrite fault gouges under *in situ* stress, pressure and temperature conditions similar to those employed in the experiments of Pluymakers *et al.* (2014). We then extrapolate our models to *in situ* conditions more directly relevant to subsurface CO_2 storage in depleted hydrocarbon reservoirs and to faults cutting the seismogenic anhydrite/carbonate cover sequence present in the Italian Apennines.

Comparison of our diffusion- and dissolution-/precipitation-controlled models for upper crustal effective stresses and temperatures corresponding to the experiments reported by Pluymakers *et al.* (8.5 MPa and 80 °C), using the parameter values shown in Table 2, demonstrates that reaction control will only become important at grain sizes below 2 μm. Increasing the effective stress to 40 MPa and the temperature to 150 °C indicates reaction control will become important only at grain sizes below about 1 μm under these conditions (using $DS = 10^{-19}$ m^3 s^{-1}, which gives the maximum value here). Natural and experimental fault gouges contain a range of grain sizes, mainly in the range 2–100 μm with over 50% of grains smaller than 10 μm (Logan *et al.* 1979; Keulen *et al.* 2007). On this basis, we propose diffusion-controlled Model D4, represented by Equation (26), as the best description of the pressure solution process in natural anhydrite gouge under upper crustal conditions, that is, the rate equation

$$\dot{\varepsilon}_{d4} = \frac{2\pi A_d Z}{Fd^3} DC_s S \frac{B - W(Be^B)}{W(Be^B)} \frac{q}{q - 2\phi},$$

where $B = -[(Z/F)q/(q - 2\phi)(\sigma_n^e \Omega/RT) + 1]$. This equation provides the most complete description of diffusion-controlled pressure solution, with the fewest assumptions. Numerical integration of this expression provides a means of estimating the approximate time required for a porosity decrease from 48% (the starting porosity for our model) to 3%, which is generally considered as the percolation threshold for a porous medium and hence the porosity at which sealing should be complete (i.e. at which all remaining porosity becomes disconnected, regardless of the permeability before reaching this threshold porosity). Note that for high porosity after reactivation it is likely other processes, such as grain fragmentation plus subsequent

Downloaded from http://sp.lyellcollection.org/ at Universiteitsbibliotheek Utrecht on October 27, 2015

rotation and translation, will most likely cause a (near-instantaneous) porosity decrease, whereas pressure solution will dominate the longer-term compaction behaviour and hence the time to sealing. For an effective stress of *c.* 10 MPa and a temperature of 80 °C (as used in our experiments), assuming pressure solution is the only process operating and taking $d = 35$ μm and $DS = 10^{-20}$ m^3 s^{-1} (in line with the asymptotic approach of the experimental data in Figure 5c towards the model predictions for this value of *DS*) and using the data shown in Table 2 for diffusion-controlled pressure solution, the estimated sealing time for an anhydrite-bearing fault is around 10 years.

However, for reservoir-bounding faults (cross-cutting the caprock) in a CO_2 storage scenario, a 10 MPa effective normal stress is relatively low, assuming hydrostatic fluid pressure (e.g. Ramm 1992) and a normal stress equal to the overburden pressure. Using parameter values in Equation (26) (Model D4) listed in Table 2 plus a temperature of 80 °C, but varying the effective normal stress between 5 and 40 MPa (corresponding to depths of 1–3.5 km), shows that sealing times decrease rapidly with increasing normal stress and thus depth (Fig. 6). Additionally, in nature fault gouges consist of a broad range of (fine) grain sizes (e.g. Logan *et al.* 1979; Keulen *et al.* 2007) which speed up compaction creep (Niemeijer *et al.* 2009) and hence fault sealing. In practice sealing should occur over a few decades or less, which is short compared to the time scales relevant for CO_2 storage (thousands of years; IPCC 2007). The implication is that even if faults in an anhydrite caprock system are reactivated during the active CO_2 injection phase, they should self-seal quickly enough to pose only a small long-term leakage risk. This will be especially so for a storage reservoir that is underpressured with CO_2 (i.e. the CO_2 pressure is less than the pore fluid pressure in the surrounding rocks), such that penetration of CO_2 into the fault gouge and possible reaction with the gouge are avoided. Similar arguments apply for geological storage of methane and hydrogen.

If faults in anhydrite formations can seal by compacting to approach the percolation threshold on time scales of a few decades and less, it is likely that fault healing or re-strengthening will

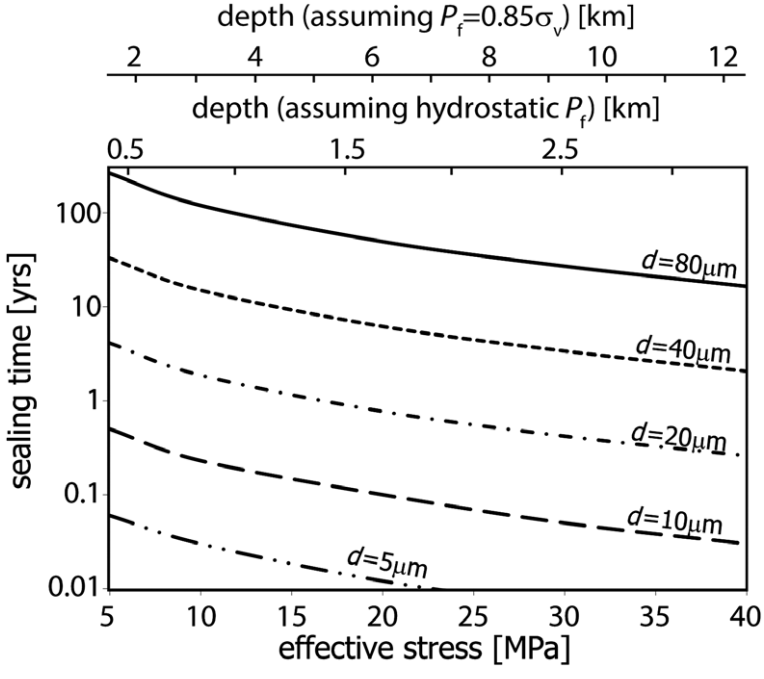

Fig. 6. Fault gouge sealing time for a porosity decrease of 48.5 → 3% (assumed to represent the percolation threshold), as predicted by diffusion-controlled model D4 for grain diameters (d) between 5 and 80 μm as a function of effective normal stress (MPa) and depth (m), at a constant temperature of 80 °C. Depth values are calculated assuming the normal stress on the fault equals the effective stress caused by the overburden pressure (σ_v). Depth values in black are representative of a storage reservoir setting, assuming a hydrostatic pore fluid pressure head, whereas depth values in grey are representative of the Italian Apennines where $P_f = 0.85\sigma_v$.

Downloaded from http://sp.lyellcollection.org/ at Universiteitsbibliotheek Utrecht on October 27, 2015

occur even more rapidly following a fault reactivation event. This has implications not only for strength evolution following fault reactivation that may occur in geological storage systems, but also in relation to natural seismicity in anhydrite-bearing terrains. In the central Apennines in Italy, many of the destructive earthquakes and aftershocks that characterize the region are known to nucleate in the interbedded carbonate/anhydrite cover sequence known as the Burano Formation. In this region, high fluid pressures related to mantle degassing (up to 85% of the lithostatic pressure) are found at seismogenic depths (Collettini & Barchi 2002; Chiodini *et al.* 2004; Miller *et al.* 2004; Trippetta *et al.* 2013), leading to relatively low normal stresses. Assuming then that the presence of Ca-sulphates in exposed faults (De Paola *et al.* 2008) indicates that faults at depth contain anhydrite, application of our pressure solution model is reasonable for the expected normal stress range and for typical fault gouge grain sizes of 10–80 μm (cf. our experiments). Consider now the model predictions of fault sealing times for a temperature of 80 °C shown as a function of effective normal stress in Figure 6. Assuming the normal stress to be lithostatic with a pore fluid pressure of 85% of lithostatic, as appropriate for the Apennines, these predictions should roughly apply for depths between *c.* 2 and 12.5 km (see upper scale, Fig. 6). Taking the temperatures expected at depths beyond 3 km, that is, higher than 80 °C into account, the fault sealing times calculated in Figure 6 will likely be overestimates, since activation of other deformation processes such as crystal plasticity will tend to speed up healing/sealing. Seismic recurrence times for major earthquakes in the Apennines region ($M \geq 5$) are of the order 2000–5000 years (Pantosti *et al.* 1993; Cello *et al.* 1997; Palumbo *et al.* 2004; Galli *et al.* 2008). This means that if anhydrite fault gouge is present within the fault cores it has the time to fully seal and heal between major ruptures, and that fault strength recovery in anhydrite-dominated faults is not the factor that controls the repeat frequency of events with $M \geq 5$. For such faults, the repeat frequency is more likely controlled by tectonic loading rate, pore fluid pressure build-up due to the natural CO_2 accumulation reported in the Apennines (Chiodini *et al.* 2004; Collettini *et al.* 2008; Walters *et al.* 2009; Ciotoli *et al.* 2013; Trippetta *et al.* 2013) or factors such as the re-strengthening behaviour of faults cutting the carbonate units present in the carbonate-anhydrite cover stratigraphy (i.e. by the behaviour of calcite and especially dolomite-rich gouges). In contrast, since earthquake repeat frequency scales with magnitude according to the Gutenberg-Richter law, anhydrite healing and sealing may well play a role for events with $M < 5$.

Conclusions

We have derived kinetic models for compaction of granular aggregates by dissolution-controlled, precipitation-controlled and diffusion-controlled pressure solution, clarifying and/or avoiding many of the assumptions made in previous work, and explicitly including the effect of aggregate porosity on strain rate. We have compared our models with the experimental results on compaction creep of wet anhydrite fault gouge, previously reported by Pluymakers *et al.* (2014). Our conclusions are as follows.

(1) Regardless of the detailed assumptions and simplifications made in deriving pressure solution models, diffusion-controlled pressure solution in anhydrite fault gouge will be rate controlling for grain sizes greater than 1–2 μm, at least for effective stresses of the order of 10–40 MPa and for upper crustal temperatures. This supports the conclusions on the experimentally determined compaction creep rates for fine-grained anhydrite fault gouge reported by Pluymakers *et al.* (2014), that is, compaction most likely occurred by diffusion-controlled pressure solution.

(2) Kinetic models for diffusion-controlled pressure solution, derived by either classical approaches (e.g. Rutter 1976) or using a dissipation approach (Lehner 1990; Spiers & Schutjens 1990), produce essentially identical predictions for the compaction creep rate of fine anhydrite fault gouges for normalized porosities (ϕ/ϕ_0) below 0.8–0.9 (i.e. absolute porosities below 40–45%), regardless of approximations generally made in these models relating to grain contact stress magnitude (low stress approximation) and grain boundary solute concentration.

(3) The most rigorous model for diffusion-controlled pressure solution derived here is based on a dissipation balance approach, applied avoiding the approximations usually made for grain boundary solute concentration as well as the assumption of low grain contact stress. This model, along with the other diffusion-controlled models considered, predicts sealing times (time to reach the percolation threshold) of up to several tens of years for faults filled with anhydrite gouge with a grain size of 5–80 μm at *in situ* upper crustal conditions.

(4) Such time scales are short compared to the time scales relevant for CO_2 storage, implying that even if faults in an anhydrite caprock system are reactivated during the CO_2 injection phase they should self-seal quickly

Downloaded from http://sp.lyellcollection.org/ at Universiteitsbibliotheek Utrecht on October 27, 2015

enough to pose only a minor long-term leakage risk, particularly if the storage reservoir is underpressured with CO_2.

(5) Since recurrences times for earthquakes with $M > 5$ in the central Apennines are 2000–5000 years, anhydrite-rich faults in this region will fully heal between these events. Fault strength recovery in anhydrite-dominated faults therefore cannot be the factor that controls this repeat frequency, though it may play a role in controlling recurrence time for (much) smaller events.

This research was performed within Work Package 3.3 (Storage) of the Dutch national carbon capture and storage research programme, CATO-2. We thank J. Penninga (Nederlandse Aardolie Maatschappij B.V.) and S. Hangx (Shell Global Solutions) for supplying the sample material. We also thank two anonymous reviewers for their constructive and most useful comments on this paper.

References

Angevine, C. L., Turcotte, D. L. & Furnish, M. D. 1982. Pressure solution lithification as a mechanism for the stick-slip behavior of faults. *Tectonics*, **1**, 151–160, doi: 10.1029/TC001i002p00151

Bildstein, O., Worden, R. H. & Brosse, E. 2001. Assessment of anhydrite dissolution as the rate-limiting step during thermochemical sulfate reduction. *Chemical Geology*, **176**, 173–189, http://dx.doi.org/10.1016/s0009-2541(00)00398-3

Blount, C. W. & Dickson, F. W. 1969. The solubility of anhydrite (CaSO4) in NaCl–H2O from 100 to 450 °C and 1 to 1000 bars. *Geochimica et Cosmochimica Acta*, **33**, 227–245, http://dx.doi.org/10.1016/0016-7037(69)90140-9

Brantley, S., Kubicky, J. & White, A. 2008. *Kinetics of Water-Rock Interaction*. Springer, New York, USA.

Cantucci, B., Montegrossi, G., Vaselli, O., Tassi, F., Quattrocchi, F. & Perkins, E. H. 2009. Geochemical modeling of CO2 storage in deep reservoirs: the Weyburn Project (Canada) case study. *Chemical Geology*, **265**, 181–197, http://dx.doi.org/10.1016/j.chemgeo.2008.12.029

Cello, G., Mazzoli, S., Tondi, E. & Turco, E. 1997. Active tectonics in the central Apennines and possible implications for seismic hazard analysis in peninsular Italy. *Tectonophysics*, **272**, 43–68, http://dx.doi.org/10.1016/S0040-1951(96)00275-2

Chang, R. 2000. *Physical Chemistry for the Chemical and Biological Sciences*. University Science Books, Sausalito, California.

Chen, J., Yang, X., Duan, Q., Shimamoto, T. & Spiers, C. J. 2013. Importance of thermochemical pressurization in the dynamic weakening of the Longmenshan Fault during the 2008 Wenchuan earthquake: inferences from experiments and modeling. *Journal of Geophysical Research: Solid Earth*, **118**, 4145–4169, http://dx.doi.org/10.1002/jgrb.50260

Chiodini, G., Cardellini, C., Amato, A., Boschi, E., Caliro, S., Frondini, F. & Ventura, G. 2004. Carbon dioxide Earth degassing and seismogenesis in central and southern Italy. *Geophysical Research Letters*, **31**, L07615, http://dx.doi.org/10.1029/2004gl019480

Ciotoli, G., Etiope, G., Florindo, F., Marra, F., Ruggiero, L. & Sauer, P. E. 2013. Sudden deep gas eruption nearby Rome's airport of Fiumicino. *Geophysical Research Letters*, **40**, 2013GL058132, http://dx.doi.org/10.1002/2013gl058132

Collettini, C. & Barchi, M. R. 2002. A low-angle normal fault in the Umbria region (Central Italy): a mechanical model for the related microseismicity. *Tectonophysics*, **359**, 97–115.

Collettini, C., Cardellini, C., Chiodini, G., De Paola, N., Holdsworth, R. E. & Smith, S. A. F. 2008. Fault weakening due to CO2 degassing in the Northern Apennines: short- and long-term processes. *In*: Wibberley, C. A. J., Kurz, W., Imber, J., Holdsworth, R. E. & Collettini, C. (eds) *The Internal Structure of Fault Zones: Implications for Mechanical and Fluid-Flow Properties*. Geological Society, London, Special Publications, **299**, 175–194, http://dx.doi.org/10.1144/sp299.11

Collettini, C., De Paola, N. & Faulkner, D. R. 2009. Insights on the geometry and mechanics of the Umbria-Marche earthquakes (Central Italy) from the integration of field and laboratory data. *Tectonophysics*, **476**, 99–109, http://dx.doi.org/10.1016/j.tecto.2008.08.013

De Meer, S. & Spiers, C. J. 1997. Uniaxial compaction creep of wet gypsum aggregates. *Journal of Geophysical Research*, **102**, 875–891, http://dx.doi.org/10.1029/96jb02481

De Meer, S., Spiers, C. J. & Nakashima, S. 2005. Structure and diffusive properties of fluid-filled grain boundaries: an in-situ study using infrared (micro) spectroscopy. *Earth and Planetary Science Letters*, **232**, 403–414, http://dx.doi.org/10.1016/j.epsl.2004.12.030

De Paola, N., Collettini, C., Faulkner, D. R. & Trippetta, F. 2008. Fault zone architecture and deformation processes within evaporitic rocks in the upper crust. *Tectonics*, **27**, TC4017, http://dx.doi.org/10.1029/2007tc002230

Den Brok, S. W. J. 1998. Effect of microcracking on pressure-solution strain rate: the Gratz grain-boundary model. *Geology*, **26**, 915–918, http://dx.doi.org/10.1130/0091-7613(1998)026<0915:eomops>2.3.co;2

Faulkner, D. l. R. & Rutter, E. H. 2001. Can the maintenance of overpressured fluids in large strike-slip fault zones explain their apparent weakness? *Geology*, **29**, 503–506, http://dx.doi.org/10.1130/0091-7613(2001)029<0503:ctmoof>2.0.co;2

Faulkner, D. R., Jackson, C. A. L., Lunn, R. J., Schlische, R. W., Shipton, Z. K., Wibberley, C. A. J. & Withjack, M. O. 2010. A review of recent developments concerning the structure, mechanics and fluid flow properties of fault zones. *Journal of Structural Geology*, **32**, 1557–1575, http://dx.doi.org/10.1016/j.jsg.2010.06.009

Galli, P., Galadini, F. & Pantosti, D. 2008. Twenty years of paleoseismology in Italy. *Earth-Science Reviews*, **88**, 89–117, http://dx.doi.org/10.1016/j.earscirev.2008.01.001

Downloaded from http://sp.lyellcollection.org/ at Universiteitsbibliotheek Utrecht on October 27, 2015

GLENNIE, K. W. 2001. Exploration activities in the Netherlands and North-West Europe since Groningen. *Netherlands Journal of Geosciences*, **80**, 33–52.

GUNDERSEN, E., RENARD, F., DYSTHE, D. K., BJØRLYKKE, K. & JAMTVEIT, B. 2002. Coupling between pressure solution creep and diffusive mass transport in porous rocks. *Journal of Geophysical Research: Solid Earth*, **107**, 2317, http://dx.doi.org/10.1029/2001jb000287

HANGX, S. J. T., SPIERS, C. J. & PEACH, C. J. 2010. Creep of simulated reservoir sands and coupled chemical-mechanical effects of CO2 injection. *Journal of Geophysical Research*, **115**, B09205, http://dx.doi.org/10.1029/2009jb006939

HICKMAN, S., SIBSON, R. & BRUHN, R. 1995. Introduction to special section: mechanical involvement of fluids in faulting. *Journal of Geophysical Research: Solid Earth*, **100**, 12 831–12 840, http://dx.doi.org/10.1029/95jb01121

HUMMEL, W., BERNER, U., CURTI, E., PEARSON, F. J. & THOENEN, T. 2002. Chemical thermodynamic database 01/01. *In*: uPublish (ed.) *Nagra/PSI*. Universal Publishers, Wettingen.

IPCC 2007. Climate change 2007: synthesis report. Summary for policymakers. *In*: CORE WRITING TEAM, PACHAURI, R. K. & REISINGER, A. (eds) IPCC, Geneva.

KEULEN, N., HEILBRONNER, R., STÜNITZ, H., BOULLIER, A. & ITO, H. 2007. Grain size distributions of fault rocks: a comparison between experimentally and naturally deformed granitoids. *Journal of Structural Geology*, **29**, 1282–1300, http://dx.doi.org/10.1016/j.jsg.2007.04.003

KOELEMEIJER, P. J., PEACH, C. J. & SPIERS, C. J. 2012. Surface diffusivity of cleaved NaCl crystals as a function of humidity: impedance spectroscopy measurements and implications for crack healing in rock salt. *Journal of Geophysical Research: Solid Earth*, **117**, B01205, http://dx.doi.org/10.1029/2011jb008627

LEHNER, F. K. 1990. Thermodynamics of rocks by pressure solution. *In*: BARBER, D. J. & MEREDITH, P. G. (eds) *Deformation Processes in Minerals, Ceramics and Rocks*. Unwin Hyman Ltd, London.

LEHNER, F. K. 1995. A model for intergranular pressure solution in open systems. *Tectonophysics*, **245**, 153–170, http://dx.doi.org/10.1016/0040-1951(94)00232-X

LITEANU, E., NIEMEIJER, A., SPIERS, C. J., PEACH, C. J. & DE BRESSER, J. H. P. 2012. The effect of CO2 on creep of wet calcite aggregates. *Journal of Geophysical Research*, **117**, 20, http://dx.doi.org/10.1029/2011JB008789

LOGAN, J. M., FRIEDMAN, M., HIGGS, N. G., DENGO, C. & SHIMAMOTO, T. 1979. Experimental studies of simulated gouge and their application to studies of natural fault zones. *In*: SURVEY, U. S. G. (ed.) *Proceedings of Conference VIII, Analysis of Actual Fault zones in Bedrock*, **79–1239**, 305–343.

MILLER, S. A., COLLETTINI, C., CHIARALUCE, L., COCCO, M., BARCHI, M. & KAUS, B. J. P. 2004. Aftershocks driven by a highpressure CO2 source at depth. *Nature*, **427**, 724–727.

MIRABELLA, F., BARCHI, M. R. & LUPATTELLI, A. 2008. Seismic reflection data in the Umbria Marche Region: limits and capabilities to unravel the subsurface structure in a seismically active area. *Annals of Geophysics*, **51**, http://dx.doi.org/10.4401/ag-3032

NIEMEIJER, A. R., SPIERS, C. J. & BOS, B. 2002. Compaction creep of quartz sand at 400–600 °C: experimental evidence for dissolution-controlled pressure solution. *Earth and Planetary Science Letters*, **195**, 261–275, http://dx.doi.org/10.1016/s0012-821x(01)00593-3

NIEMEIJER, A. R., ELSWORTH, D. & MARONE, C. 2009. Significant effect of grain size distribution on compaction rates in granular aggregates. *Earth and Planetary Science Letters*, **284**, 386–391.

OIL AND GAS JOURNAL 2013. Worldwide look at reserves and production. *In*: TIPPEE, B. J. (ed.) *Oil and Gas Journal*, **110**, Series volume 12, 28–31.

PALUMBO, L., BENEDETTI, L., BOURLES, D., CINQUE, A. & FINKEL, R. 2004. Slip history of the Magnola fault (Apennines, Central Italy) from 36Cl surface exposure dating: evidence for strong earthquakes over the Holocene. *Earth and Planetary Science Letters*, **225**, 163–176, http://dx.doi.org/10.1016/j.epsl.2004.06.012

PANTOSTI, D., SCHWARTZ, D. P. & VALENSISE, G. 1993. Paleoseismology along the 1980 surface rupture of the Irpinia Fault: implications for earthquake recurrence in the southern Apennines, Italy. *Journal of Geophysical Research: Solid Earth*, **98**, 6561–6577, http://dx.doi.org/10.1029/92jb02277

PATERSON, M. S. 1973. Thermodynamics and its geological applications. *Reviews of Geophysics*, **11**, 355–389.

PATERSON, M. S. 1995. A theory for granular flow accommodated by material transfer via an intergranular fluid. *Tectonophysics*, **245**, 135–151, http://dx.doi.org/10.1016/0040-1951(94)00231-W

PLUYMAKERS, A. M. H., PEACH, C. J. & SPIERS, C. J. 2014. Diagenetic compaction experiments on simulated anhydrite fault gouge under static conditions. *Journal of Geophysical Research: Solid Earth*, **119**, 4123–4148.

RAJ, R. 1982. Creep in polycrystalline aggregates by matter transport through a liquid phase. *Journal of Geophysical Research*, **87**, 4731–4739, http://dx.doi.org/10.1029/JB087iB06p04731

RAMM, M. 1992. Porosity-depth trends in reservoir sandstones: theoretical models related to Jurassic sandstones offshore Norway. *Marine and Petroleum Geology*, **9**, 553–567, http://dx.doi.org/10.1016/0264-8172(92)90066-N

RENARD, F., ORTOLEVA, P. & GRATIER, J. P. 1997. Pressure solution in sandstones: influence of clays and dependence on temperature and stress. *Tectonophysics*, **280**, 257–266.

RUTQVIST, J., RINALDI, A. P., CAPPA, F. & MORIDIS, G. J. 2013. Modeling of fault reactivation and induced seismicity during hydraulic fracturing of shale-gas reservoirs. *Journal of Petroleum Science and Engineering*, **107**, 31–44, http://dx.doi.org/10.1016/j.petrol.2013.04.023

RUTTER, E. H. 1976. The kinetics of rock deformation by pressure solution. *Philosophical Transactions of the Royal Society of London. Series A, Mathematical and Physical Sciences*, **283**, 203–219.

RUTTER, E. H. 1983. Pressure solution in nature, theory and experiment. *Journal of the Geological Society*,

Downloaded from http://sp.lyellcollection.org/ at Universiteitsbibliotheek Utrecht on October 27, 2015

140, 725–740, http://dx.doi.org/10.1144/gsjgs.140.5.0725

SCHUTJENS, P. T. M. 1991. Experimental compaction of quartz sand at low effective stress and temperature conditions. *Journal of the Geological Society London*, **148**, 527–539, http://dx.doi.org/10.1144/gsjgs.148.3.0527

SCHUTJENS, P. T. M. & SPIERS, C. J. 1999. Intergranular pressure solution in Nacl: grain-to-grain contact experiments under the optical microscope. *Oil & Gas Science and Technology*, **54**, 729–750, http://dx.doi.org/10.2516/ogst:1999062

SHIMIZU, I. 1995. Kinetics of pressure solution creep in quartz: theoretical considerations. *Tectonophysics*, **245**, 121–134, http://dx.doi.org/10.1016/0040-1951(94)00230-7

SIBSON, R. H. 1992. Implications of fault-valve behaviour for rupture nucleation and recurrence. *Tectonophysics*, **211**, 283–293, http://dx.doi.org/10.1016/0040-1951(92)90065-E

SPIERS, C. J. & SCHUTJENS, P. T. M. 1990. Densification of crystalline aggregates by fluid-phase diffusional creep. *In*: BARBER, D. J. & MEREDITH, P. G. (eds) *Deformation Processes in Minerals, Ceramics and Rocks*. Unwin Hyman Ltd, London.

SPIERS, C. J., DE MEER, S., NIEMEIJER, A. R. & ZHANG, X. 2004. Kinetics of rock deformation by pressure solution and the role of thin aqueous films. *In*: NAKASHIMA, S., SPIERS, C. J., MERCURY, L., FENTER, P. A. & HOCHELLA, M. F., JR. (eds) *Physicochemistry of Water in Geological and Biological Systems – Structures and Properties of Thin Aqueous Films*. Universal Academy Press, Inc., Tokyo, 129–158.

THOENEN, T. & KULIK, D. 2003. Chemical thermodynamical database 01/01 for the GEM-Selektor (V.2-PSI). *In*: PSI (ed.) *Geochemical Modeling Code*. Villigen, LES PSI Thermodynamics Group.

TRIPPETTA, F., COLLETTINI, C., VINCIGUERRA, S. & MEREDITH, P. G. 2010. Laboratory measurements of the physical properties of Triassic Evaporites from Central Italy and correlation with geophysical data. *Tectonophysics*, **492**, 121–132, http://dx.doi.org/10.1016/j.tecto.2010.06.001

TRIPPETTA, F., COLLETTINI, C., BARCHI, M. R., LUPATTELLI, A. & MIRABELLA, F. 2013. A multidisciplinary study of a natural example of a CO2 geological reservoir in central Italy. *International Journal of Greenhouse Gas Control*, **12**, 72–83, http://dx.doi.org/10.1016/j.ijggc.2012.11.010

VAN NOORT, R. & SPIERS, C. J. 2009. Kinetic effects of microscale plasticity at grain boundaries during pressure solution. *Journal of Geophysical Research: Solid Earth*, **114**, B03206, http://dx.doi.org/10.1029/2008jb005634

VANDEWEIJER, V., VAN DER MEER, B., HOFSTEE, C., MULDERS, F., D'HOORE, D. & GRAVEN, H. 2011. Monitoring the CO2 injection site: K12-B. *Energy Procedia*, **4**, 5471–5478, http://dx.doi.org/10.1016/j.egypro.2011.02.532

WALTERS, R. J., ELLIOTT, J. R. *ET AL*. 2009. The 2009 L'Aquila earthquake (central Italy): a source mechanism and implications for seismic hazard. *Geophysical Research Letters*, **36**, L17312, http://dx.doi.org/10.1029/2009gl039337

WIBBERLEY, C. A. J. & SHIMAMOTO, T. 2003. Internal structure and permeability of major strike-slip fault zones: the Median Tectonic Line in Mie Prefecture, Southwest Japan. *Journal of Structural Geology*, **25**, 59–78, http://dx.doi.org/10.1016/S0191-8141(02)00014-7

WIBBERLEY, C. A. J., YIELDING, G. & DI TORO, G. 2008. Recent advances in the understanding of fault zone internal structure: a review. *In*: WIBBERLEY, C. A. J., KURZ, W., IMBER, J., HOLDSWORTH, R. E. & COLLETTINI, C. (eds) *The Internal Structure of Fault Zones: Implications for Mechanical and Fluid-Flow Properties*. Geological Society, London, Special Publications, **299**, 5–33, http://dx.doi.org/10.1144/sp299.2

ZHANG, X. & SPIERS, C. J. 2005. Compaction of granular calcite by pressure solution at room temperature and effects of pore fluid chemistry. *International Journal of Rock Mechanics and Mining Sciences*, **42**, 950–960.

ZHANG, X., SPIERS, C. J. & PEACH, C. J. 2010. Compaction creep of wet granular calcite by pressure solution at 28 °C to 150 °C. *Journal of Geophysical Research*, **115**, B09217, http://dx.doi.org/10.1029/2008jb005853